Innovative Infrastructure Solutions (2021) 6:56
https://doi.org/10.1007/s41062-020-00411-x

TECHNICAL PAPER

Field study on axial behavior of instrumented post-grouted steel pipe micropiles in tropical lateritic soil

Luiz Felipe Goulart Fiscina[1] · Yuri Barbosa[1] · Paulo José Rocha de Albuquerque[1] · David de Carvalho[2]

Received: 24 August 2020 / Accepted: 18 November 2020 / Published online: 12 January 2021

Abstract

This paper presents a field study on the axial behavior of new configuration of steel pipe micropiles in tropical lateritic soil. The micropiles were installed following a two-step grouting process with high injection pressures at a new experimental site located at the University of Campinas (Unicamp). The main innovation of the micropiles relies on the use of high-strength steel pipes as a drilling tool, casing protection, structural component and injection device. Full-scale pile loading tests were performed under compression and tension loads to investigate the axial behavior of the micropiles. The micropiles were instrumented along the shaft with electrical extensometers, and they were monitored during the progress of the loading tests. The load–movement responses, elastic moduli, axial load transfer mechanism, and unit bond stress relating to the micropiles and their interactions with the tropical soil were measured and evaluated. The bearing capacity of the post-grouted micropiles was considerably improved by the proposed post-grouting technique. The ultimate load capacity of the grouted steel pipe micropile under a compression load is approximately the same under a tension load. The average ultimate bond strength was 99 kPa and 100 kPa for the micropile under compression and tension, respectively. The distribution of unit bond stress along the shaft of the micropile under compressive and tensile load presented a post-peak softening behavior. The average ultimate grout-to-ground strength at the soil–micropile interface was 2.4 and 1.7 times greater than other nongrouted and non-injected piles installed in the same soil conditions at Unicamp.

Keywords Post-grouted micropiles · Tropical lateritic soil · Axial bearing capacity · Field test · Load–movement response · Grout-to-ground bond strength

Introduction

Micropiles are drilled and grouted deep foundation elements, heavily reinforced with a nominal diameter less than 300 mm [1]. They were conceived in Italy in the 1950s by the Italian civil engineer, Prof. Eng. Fernando Lizzi [2]. The technology was a breakthrough in the deep foundation market and quickly spread around the world [3]. Their first applications were for the direct structural underpinning of old structures as an innovative solution to rebuild and reinforce old buildings affected by the post-war effects [4]. With the micropiles technology outbreak in the global market after the 1980s, there was also an increase in the number of construction methodologies regarding them [5]. They basically vary from the type of grouting methodology to be performed and their design application [1]. According to this code, there are at least four types of grouting methodologies: type A, in which grout is placed by gravity with no injection pressure; type B, in which grout is placed by gravity and the injection pressure (between 0.5 and 1 MPa) is applied at the top of the micropile while the case is withdrawn; type C, in which grout is placed by gravity and, after its hardening, a similar grout is injected under the pressure of about 1 MPa through a sleeved grout pipe; and type D,

✉ Luiz Felipe Goulart Fiscina
l226664@dac.unicamp.br

Yuri Barbosa
y209352@dac.unicamp.br

Paulo José Rocha de Albuquerque
pjra@unicamp.br

David de Carvalho
david@feagri.unicamp.br

[1] School of Civil Engineering, Architecture and Urban Design, University of Campinas (Unicamp), 224, Saturnino de Brito St., Campinas, São Paulo 13083-889, Brazil

[2] School of Agriculture Engineering, University of Campinas, Campinas, São Paulo, Brazil

similar to type C, but with one or more additional phases of grout injection (higher than 2 MPa) using a double packer in the desired depths. Types C and D are also called post-grouting techniques. The design application of micropiles in the current scenario includes solutions to a diverse range of engineering problems such as underpinning existing foundations [6–11], seismic retrofitting [12–15] and in situ reinforcement [16–20]. In terms of geotechnical capacity, it is widely assumed that the geotechnical capacity of micropiles under axial loading is mainly governed by the grout-to-ground bond strength along the shaft, especially for workload conditions [5]. Moreover, longer duration of grouting injection, i.e., higher cement consumption, can lead to higher values of bearing capacity [21] as well as the use of post-grouting techniques [22–26]. Field tests such as those conducted by Gómez et al. [27], Seo et al. [28] and Jang and Han [29] suggest that even when micropiles are embedded in a competent stratum, the load transfer mechanism is governed by the grout-to-ground bond resistance. Thus, tip resistance is usually neglected because of the relatively small cross-sectional area of the pile and the uncertainties regarding the presence of loose soil immediately below the pile tip after the drilling process [5]. The FHWA [1] provides guidance on the ultimate grout-to-ground bond strength values (α_{bond}) for preliminary designs for each type of micropile (A, B, C and D) and soil profile. These values were developed based on the experience of several authors and published information on drilled shafts, soil nails and tiebacks. This method considers that the shaft resistance of micropiles under compression or tension loads is of the same magnitude, even though field studies prove that the compression shaft resistance is usually greater than the tension shaft resistance [30–32]. Although the bearing capacity and the load transfer characteristics of micropiles embedded in cohesive and cohesionless soils have been extensively studied by means of experimental tests in the last two decades [27, 28, 30, 32–36], there are little published data on the behavior of micropiles submitted to axial load in tropical lateritic soils [37, 38]. Furthermore, the majority of field tests cover the type A [27, 28, 39], the type B [8, 21, 29, 36] and the type C [31, 32, 39] grouting classifications according to FHWA [1] which leads to a lack of field studies on the axial behavior of type D micropiles. It is well known that instrumented load tests are the most effective alternative to obtain more reliable project parameters, especially in the case of micropiles, since the parameters suggested by FHWA [1] could result in an underestimation of the actual micropile geotechnical capacity [35, 36, 40]. Cadden et al. [5] emphasized that the lack of detailed measurements of the limit bond strength of types *C* and *D* micropiles has resulted in conservatives values and, in order to overcome this issue, development of a more complete database on ultimate geotechnical bond strength obtained by instrumented static load tests installed in different geological site conditions is necessary. Hence, the aim of this paper is to investigate the load–movement responses and the grout-to-ground bond strength of a new configuration of post-grouted (type *D*) steel pipe micropiles under axial loads and embedded in a tropical lateritic soil. Aspects such as the load-transfer mechanisms, the difference between compressive and tensile loads on post-grouted micropiles are evaluated and discussed. The ultimate bond strength measured in the field was compared with the range of values proposed by the FHWA [1] to verify whether this methodology offers proper results for preliminary design in tropical soils. Finally, the influence of the post-grouting treatment on the grout-to-ground bond strength enhancement was evaluated and discussed.

Geotechnical site conditions

A specific testing site was created in University of Campinas—Unicamp, solely for this research. The Unicamp is in the State of São Paulo, in the city of Campinas—Brazil. It is noteworthy that Unicamp has already two other experimental sites where research has been carried out into the soil–pile behavior of various types of foundation performed in a typical soil of the region (tropical diabase soil). As a result, several papers were published in international journals [41–44], recognized international conferences [45–49] and book chapters [50]. All of them contributed significantly to the overall understanding of the geotechnical and geological characteristics of the inherent tropical soil of the region. Figure 1 presents the location of each experimental site at Unicamp according to a Google Earth aerial photograph.

Regarding the new experimental site, a campaign of two Piezocone Penetration Tests (CPTu) and five Standard Penetration Tests (SPT) was performed to characterize the site conditions. The soil stratigraphy interpreted from the SPT and CPTu results is given in Fig. 2. A top layer of reddish clayey silt (colluvium soil) of about 5 m thick overlays a large deposit of a mixed clay material (diabase residual soil) horizon down to 20 m. Lenses of lateritic concretions were observed in the form of peak values of cone resistance throughout the CPTu test. These lenses were also found in the studies conducted by Albuquerque et al. [41]. The undrained shear resistance (Su) was obtained directly from the CPTu tests according to Eq. (1), proposed by Robertson [51].

$$\mathrm{Su} = \frac{q_t - \sigma_{vo}}{N_{kt}} \quad (1)$$

where q_t is the corrected cone tip resistance, σ_{vo} is the effective stress and N_{kt} is a cone factor with an average value of 14. The N values of the Standard Penetration Tests ($N_{SPT,60}$)

Fig. 1 Location of each experimental site at Unicamp

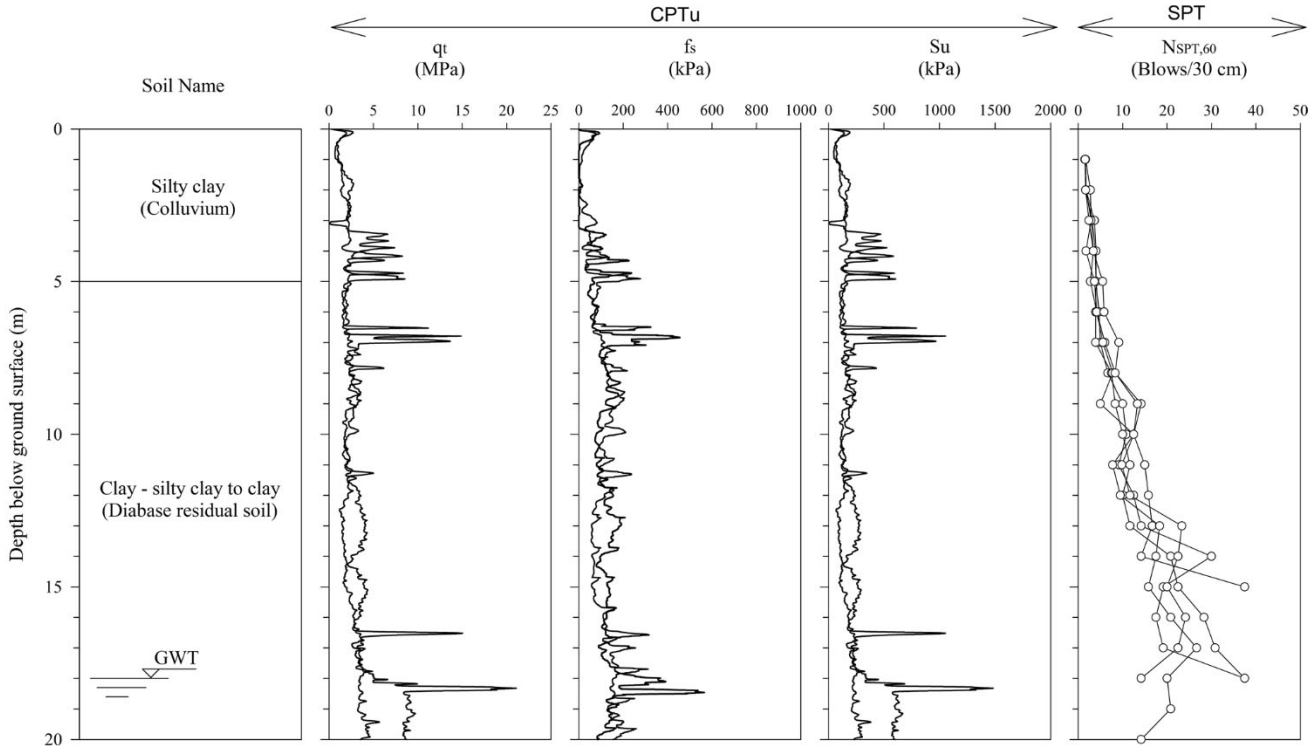

Fig. 2 Physical and mechanical properties of the layered soil at the new experimental site

remain approximately constant ($N_{SPT} = 4$) up to 5 m below the ground level and rises to a value between 10 and 30 at higher depths. The Atterberg limits tests, from the SPT soil samples, presented a value of liquid limit (LL) and plasticity index (PI) varying from 50 to 58% and 11% and 15%, respectively. Therefore, according to the Unified Soil Classification System [52], the in situ soil can be classified as a high-plasticity silt (MH). The groundwater table (GW)

was found at a depth of 18 m below the surface. Finally, the in situ test results revealed that the new site has similar geological conditions when compared to the two other experimental fields at Unicamp.

Micropile installation and materials

The new configuration of micropiles object of this study may be classified as a type *D* according to the micropile classification method suggested by the FHWA [1]. They were performed with a total length of 17 m and a nominal diameter of 0.30 m. Furthermore, the steps regarding the micropiles installation are summarized as follows:

1. Soil drilling was performed by rotary equipment connected to steel pipes with internal water circulation. The casing tube has a structural function, and it is composed of several 8″-diameter (200 mm) N-80 steel pipe sections with a length of 2.5 m each and threads at their ends for connection between male and female joints. They also contain a special Manchette system along its length for grout injection purposes. The Manchette valves are spaced 0.5 m apart in each steel pipe section, and their structure is composed of an aluminum body and a packer rubber that opens with an injection pressure of approximately 2.0 MPa and automatically closes after the pressure is removed, avoiding the neat cement grout and/or loose soil to flow back into the pile. Finally, the first section of the pipe has a crown for drilling, and, in case of resistant bearing stratum, eccentric bits with Widia components can be inserted inside the steel pipe in order to decompose the resistant soil layer with the aid of water percolation. The present study used this device in order to overcome the lenses of lateritic concretions and the resistant ground stratum at deep soil layers;
2. Once the target depth had been reached, a single packer was placed inside the steel pipe, at the bottom of the excavation, to start the preliminary treatment. The packer was then inflated by the support of a hydraulic pump with the objective to seal the tip of the pile. Afterward, the neat cement grout was injected (injection pressure from 1.8 to 2.0 MPa) by a PVC tube internally connected to the single packer until it started to overflow at the top of the micropile with a clean aspect, i.e., without any apparent loose soil particle. The grout used had a water cement ratio (W/C) of 0.5 supplied by a grout plant. The main purpose of this treatment is to wash loose material out of the soil/pile interface and inject cement grout from bottom to top in order to fulfill the annulus space between the out diameter of the micropile and the surrounding soil (annulus grout);
3. The post-grouting phase was performed at least 12 h after the first phase. A double packer was inserted at the last Manchette of the micropile, located near the tip and then inflated to seal the region which was intended to be treated. Neat cement grout ($W/C = 0.5$) was then injected by the same system described in the last phase at a pressure of 2.1–2.6 MPa. When the grouting was completed or if the Manchette valve could not be open, the double packer would be moved to the next upper valve to repeat the process. All Manchette valves underwent the post-grouting phase. Some of them were able to open, while others could not. Details about the grouting operation are presented in Table 1;
4. Lastly, the interior of the tube was filled with grout from bottom to top. Figure 3 presents the main features used during the micropiles installation, and Fig. 4 summarizes all phases aforementioned.

As the MT micropile was submitted to a tensile static loading test, it had an additional installation phase between

Table 1 Main aspects of the grouting operation

Pile	Pile segment (m)	N.V.[c]	Soil description	P.T.[d] (kg/MPa)	F.P.[e] (kg)	V.O.F.[f]	S.P.[g] (kg)	V.O.S.[h]	A.I.G.P.[i] (MPa)	A.R.P.G.[j] (MPa)
MC[a]	0–5	8	Silty clay	1200/2.0	–	–	–	–	–	–
	5–11.6	15	Clay—silty clay to clay		950	11	–	–	2.5	1.7
	11.6–17	11	Clay—silty clay to clay		700	4	–	–	2.1	1.7
MT[b]	0–5	8	Silty clay	1200/1.8	–	–	–	–	–	–
	5–11.6	15	Clay—silty clay to clay		600	7	–	–	2.4	1.8
	11.6–17	11	Clay—silty clay to clay		900	8	950	5	2.6	1.9

[a]MC = micropile under compression loads; [b]MT = micropile under tension loads; [c] N.V. = number of valves of the pile segment; [d]P.T. = preliminary treatment cement consumption (kg)/average injection pressure (MPa); [e]F.P. = first post-grouting treatment cement consumption; [f]V.O.F. = number of valves which opened in the first post-grouting treatment; [g]S.P. = second post-grouting treatment cement consumption; [h]V.O.S. = number of valves which opened in the second post-grouting treatment; [i]A.I.G.P. = average grout pressure required to open the Manchette valves; [j]A.R.P.G. = average residual grout pressure to maintain the Manchette valve open

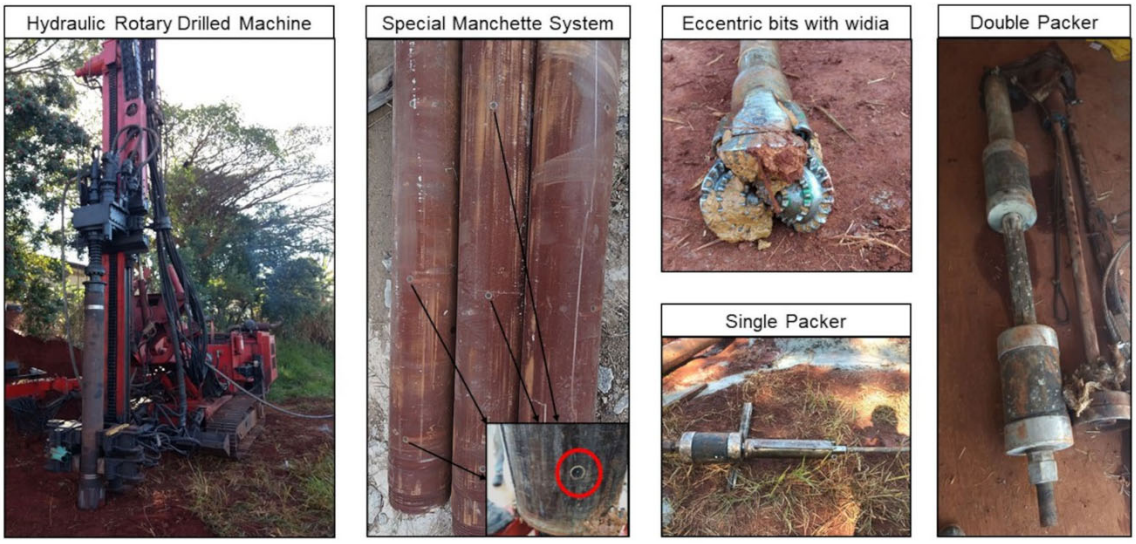

Fig. 3 Main features used during the micropiles installation

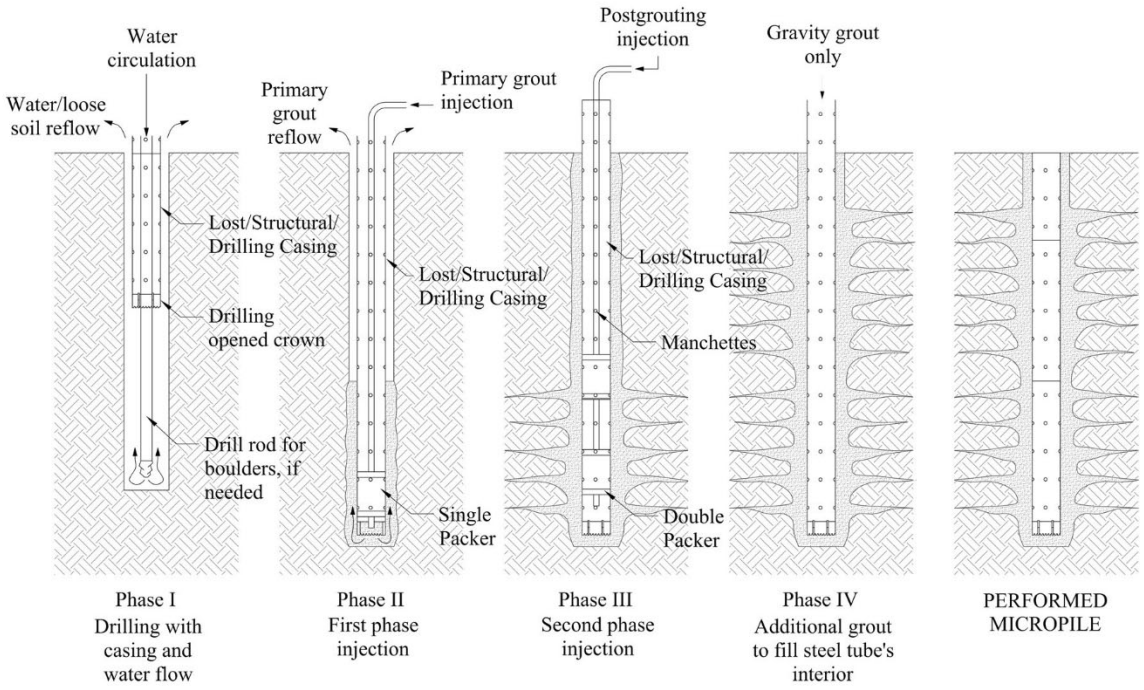

Fig. 4 Micropile installation phases

the previously mentioned steps III and IV. To make the test possible, ten 2-m-long INCO 100D threaded bars with a nominal diameter of 69 mm were inserted centrally into the casing steel tube. It is worth noting that instrumented "sister" bars were also installed between steps III and IV in both micropiles. The average section of both types of micropiles and their main components are shown in Fig. 5.

Samples of the neat cement grout were collected during the installation of each micropile. The samples' mold had a diameter of 5 cm and 10 cm in height, and all of them were immersed in water. The cylinders were tested after 28 days under compression and splitting tensile strength. Some of them were instrumented with strain gauges in order to obtain the grout elastic modulus. The average unconfined compressive and splitting strength was 15 MPa and 2.3 MPa, respectively, while the average secant elastic modulus was equal to 6 GPa. All specimens presented a high degree of shrinkage (total contraction of 20% of the mold's height).

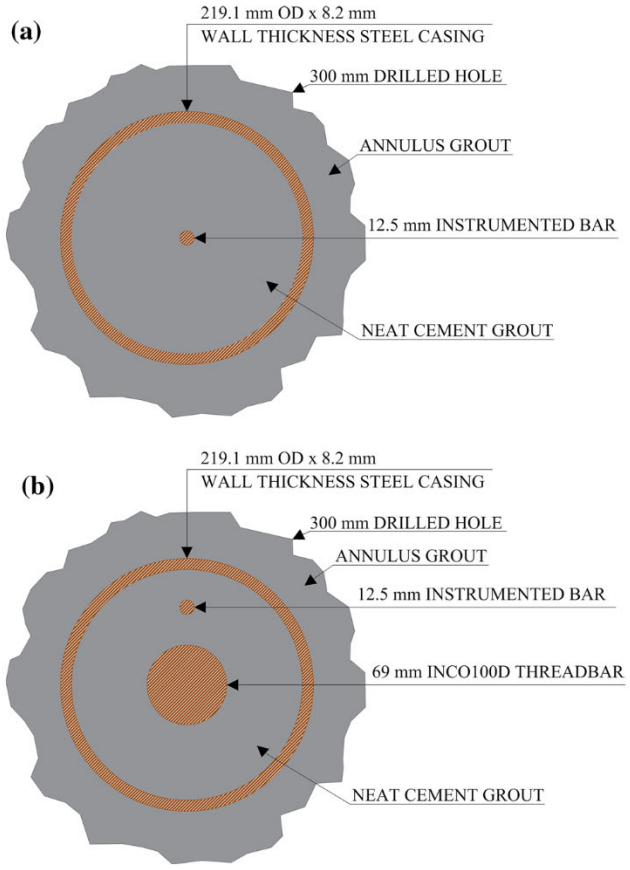

Fig. 5 Average section and main components for **a** compression micropile—MC and **b** tension micropile—MT

It should be pointed out that no admixtures were used such as superplasticizer or anti-shrinkage. Details regarding the average values of the cross-section area, drilling diameter and strength characteristics of the components of the micropile are summarized in Table 2.

Instrumentation, test setup and methods

The micropiles instrumentation was performed from a set of CA-50 steel bars, usually called "sister" bars, with a diameter of 12.5 mm and 0.6 m in length, on which surface electric strain gauges were installed. At the experimental site, the "sister" bars were connected to others of the same material with varying lengths as they were placed inside the steel casing pipe. The connections between the bars were performed with a threaded system at the end of each bar alongside steel gloves. To ensure the centricity of the instrumentations in the piles, steel centralizers were used at the tip of the pile. The preset total length of the instrumentation setup of the MC micropile had to be changed due to the presence of a stiff material near the tip level so that the reference section (first instrumented bar) was not placed outside of the steel pipe micropile. This material was likely to be related to the neat cement grout of the preliminary treatment that somehow flowed back into the steel pipe during the second phase of the installation process and consolidated in this region. Hence, the last "sister" bar was placed above the tip of the pile, at a depth of 15.8 m. In this instance, the axial load transfer diagram was extrapolated to a depth of 17 m. It is worth mentioning that as the micropile under tension loads does not develop tip resistance, tip instrumentation is not

Table 2 Geometrical and strength characteristics of the micropile components

Characteristics	Values
Borehole drilling diameter[a] (cm)	30
Borehole drilling cross-section area[a] (cm^2)	706.9
Outside diameter of the steel casing pipe[b] (cm)	21.91
Inside diameter of the steel casing pipe[b] (cm)	20.27
Cross-section area of the steel casing pipe[b] (cm^2)	54.33
Yielding strength of the steel casing pipe in compression[b] (MPa)	655
Yielding strength of the steel casing pipe in tension[b] (MPa)	689
Yielding strength of the INCO 100D threaded bars in tension[b] (MPa)	521
Cross-section area of the INCO 100D threaded bars[b] (cm^2)	37
Young's modulus of the steel casing pipe[b] (GPa)	205
Inside cross-section area of the neat cement grout[a] (cm^2)	322.7
Annulus grout thickness[a] (cm)	4
Neat cement grout cross-section area with annulus grout[a] (cm^2)	652.5
Average unconfined compressive strength in 28 days[c] (MPa)	15
Average flexural tensile strength in 28 days[c] (MPa)	2.3
Average secant grout modulus in 28 days[c] (GPa)	6

[a]Dimensions measured in the experimental site; [b]dimensions provided by the manufacturer company; [c]tested samples

mandatory for the load transfer analysis. The resulting stress at the tip of a tension micropile for each load increment is considered irrelevant as observed by Misra and Chen [53], Misra et al. [54] and Han and Ye [30]. As a result, the load distribution from a depth of 11.6 to 17 m was estimated considering a stress level at the tip of the pile equal to zero. Figure 6 shows the final position of each instrumentation level of the micropiles studied in this paper and the regions where the Manchette valves were opened in the post-grouting phase.

A proper reaction system was designed to ensure safety during the static loading tests since high loading conditions were expected. It was basically composed of: (1) a set of reaction steel beams with allowable structural capacity up to 3000 kN; (2) a set of four micropiles to respond to the compression test load requirements; (3) a set of two micropiles which were used as support for the uplift test load requirements; and (4) auxiliary items such as steel plates and threads which were used to ensure the level of the reaction system and the connection between the threaded bars, respectively. Figure 7 illustrates a plan view of the reaction arrangement, while Fig. 8 presents a typical setup of the micropiles under compression and tension.

Compression and tension static load tests were performed on the micropiles according to the Brazilian Standard [55] to investigate the axial behavior of the micropiles. The slow maintained load test (SMLT) method was adopted, which is the standard procedure in Brazil. In summary, it consists of the following processes: (1) the load shall be applied at successive stages with a value lesser than 20% of the predicted pile workload and maintained

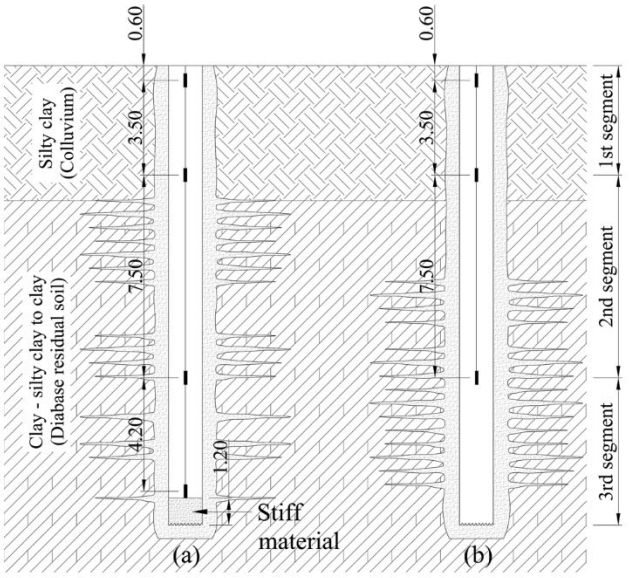

Fig. 6 Instrumentation levels for **a** compression micropile—MC and **b** tension micropile—MT

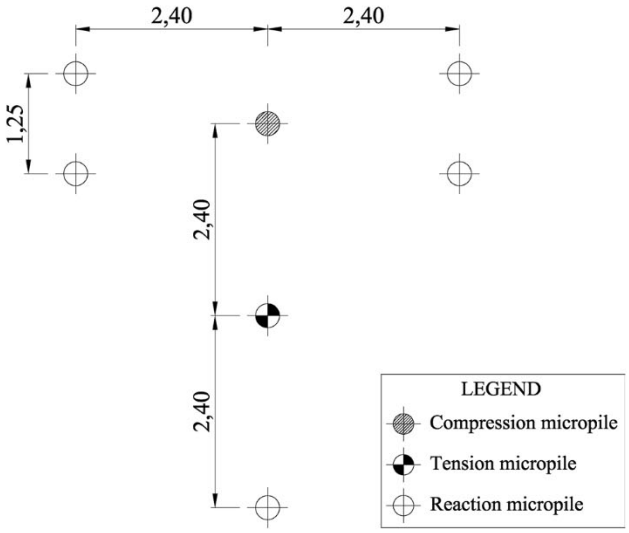

Fig. 7 Plan view of the reaction arrangement

until the stabilization of the pile head movement, with a minimum duration of 30 min; (2) the total movement in each stage must be measured and noted after 2, 4, 8, 15 and 30 min (mandatory) or until stabilization is achieved; (3) settlement stabilization may be considered set when the difference between two consecutive readings is equal to or less than 5% of the total movement of the corresponding stage; (4) at the end of the last loading stage, the maximum load must be maintained for at least 12 h before the unloading phase begins; (5) unloading shall be carried out in a minimum of four stages associated with their stabilization in the same manner of the loading phase. For the unloading phase, the total movement in each stage must be measured and noted after 2, 4, 8 and 15 min (mandatory) or until stabilization is achieved; and (6) displacement measures should be maintained until stabilization even after full pile unloading.

The loading stages carried out in the present paper were performed with increments of 100 kN. Additionally, all measurements such as the applied load, movements at the top of the pile and the instrumentation data from the instrumented bars were obtained through HBM's QuantumX Assistant 840 data acquisition system alongside a read transduction software named Catman Easy. The micropiles' head movement was monitored by four linear variable differential transformer (LVDT's), with 100 mm linear stroke and 0.01 mm accuracy, coupled in two parallel steel beams used as a support structure. They were installed at the edges of the pile cap during the SMLT. Two devices were used for the loading-level readings: a high-pressure electric hydraulic pump and a 3000 kN load cell. Figure 9 presents a schematic view of the main features used in the loading tests.

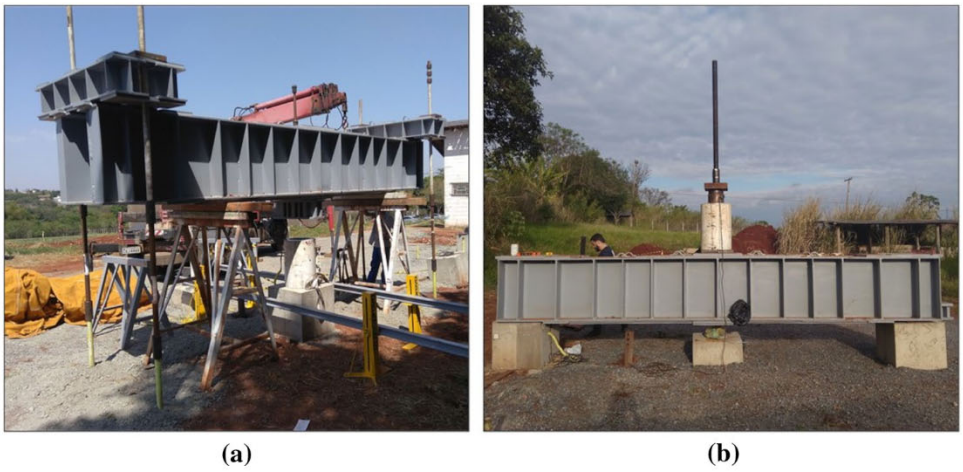

Fig. 8 Typical test setup for **a** compression micropile—MC and **b** tension micropile—MT

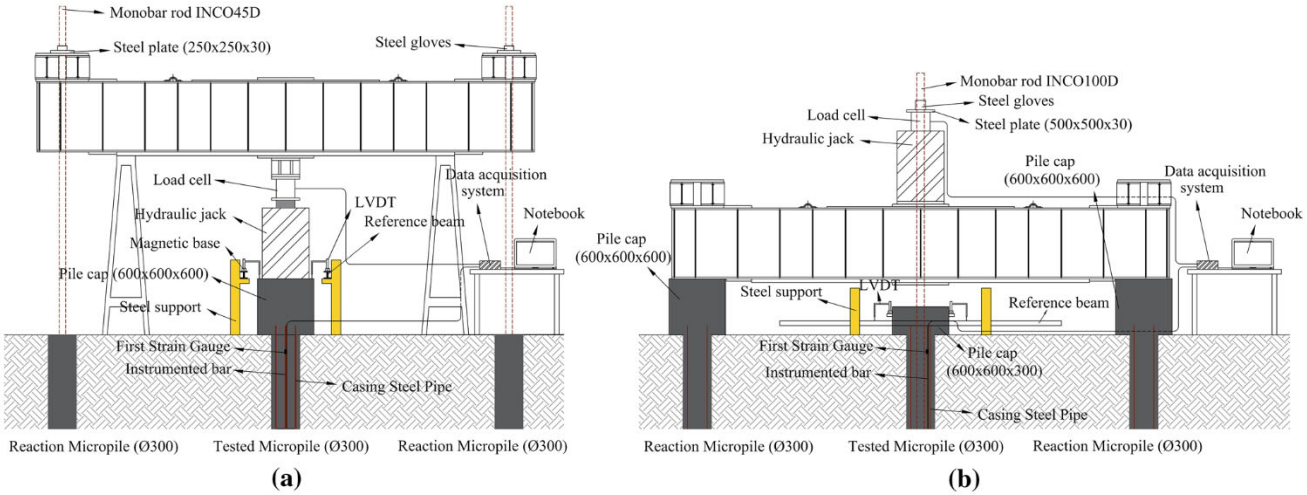

Fig. 9 Main features used in the SMLT for **a** compression micropile—MC and **b** tension micropile—MT

Axial design considerations

The micropile allowable geotechnical capacity (PG_{alw}) was calculated using Eq. (2), as suggested by the FHWA [1]:

$$PG_{alw} = \frac{\alpha_{bond}}{FS} \times \pi \times D_b \times L_b \quad (2)$$

where α_{bond} is the grout-to-ground ultimate bond strength (under compression or tension loads), FS is the factor of safety, D_b is the diameter of the drill hole and L_b is the bond length. The pile bond length of both micropiles was considered equal to the total length of the micropile, i.e., around 17 m, and their diameter equals the diameter of the drill hole ($D_b = 30$ cm). The α_{bond} adopted in this paper was the average value among the range of 50–145 kPa suggested by the FHWA [1] for silt and clay mixtures with soft to medium consistency for both representative soil layers. Therefore, the micropile allowable geotechnical capacity under compression or tension was estimated as being equal to 781 kN at a length of 17 m considering a safety factor of 2.0. The ultimate structural compression and tension loads of the micropiles were calculated to examine the structural stability during the load test. FHWA [1] suggests that the maximum load in a static load test should not exceed 80% of the ultimate structural capacity of the micropile. Thus, the ultimate capacities for compression (PSC_{ult}) and tension (PST_{ult}) load were calculated using Eqs. (3) and (4), as suggested by FHWA [1]:

$$PSC_{ult} = 0.85 f_{c,grout} A_{grout} + f_{y,casing} A_{casing} \quad (3)$$

$$PST_{ult} = f_{y,steel} \left(A_{casing} + A_{bar} \right) \quad (4)$$

where $f_{c,grout}$ is the unconfined compressive strength of the grout (28-day strength), A_{grout} is the cross-sectional area of

the grout in micropile cross section (inside casing only, discount grout outside the casing), $f_{y,casing}$ is the yield stress of the steel pipe casing, A_{casing} is the cross-sectional area of steel pipe casing, $f_{y,steel}$ is the minimum yield stress between the threaded bar and casing, A_{bar} is the cross-sectional area of steel threaded bar (centrally placed). The values regarding the strength and the geometric parameters used in Eqs. (3) and (4) can be seen in Table 2. Finally, a summary of the micropile axial design considerations is presented in Table 3.

Load test results and analysis

Load–movement responses

The load–movement responses of the micropile under compression and tension are shown in Fig. 10. The micropile under compression load presented a slightly higher load capacity than the micropile under tension load. This is probably because of the development of tip resistance for the micropile under compression loads. Similar experience was evidenced by Carvalho et al. [37] and Han and Ye [8] for type B micropiles and by Quian and Lu [31] and Wen et al. [32] for type C micropiles. The ultimate capacity of the MC micropile was 1700 kN with a total head movement of 20 mm, according to the first plunging failure. Two more attempts of load stage increment were made. However, whenever the load reached a value of approximately 1.350 kN, the pile developed a sudden new failure associated with significant deformations. After the third plunging failure, the micropile was progressively discharged to a zero-load level and the test was declared finished. The ultimate capacity of the MT micropile was 1600 kN with a total head movement of the same magnitude of the micropile under compression loads, based on the first plunging failure. It is noteworthy that the pile failed abruptly lifting the pile cap under this loading stage (pullout failure). When the reaction system was stabilized, there was one more attempt to increase the load level. In this instance, a new sudden failure happened at the load stage of 1300 kN with considerable deformations. To ensure the safety on the site, the micropile was progressively discharged to a zero-load level and the test was declared concluded.

Table 3 Micropile axial design considerations

Micropile	PG_{alw} (kN)	PG_{ult} (kN)	$PS_{ult\ (kN)}$
MC	781	1562	3970
MT	781	1562	4758

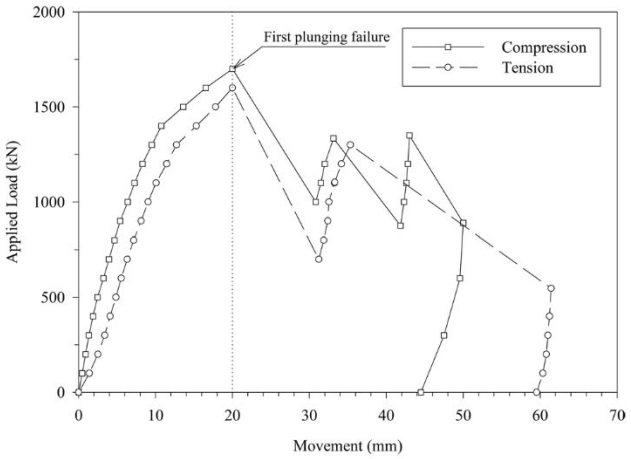

Fig. 10 Load–movement response for both compression and tension static load test

Instrumentation data and axial load transfer

Figure 11 presents the stress–strain responses of the micropiles cross-section area as recorded by the strain gauges at the four instrumented levels. What is striking about Fig. 11

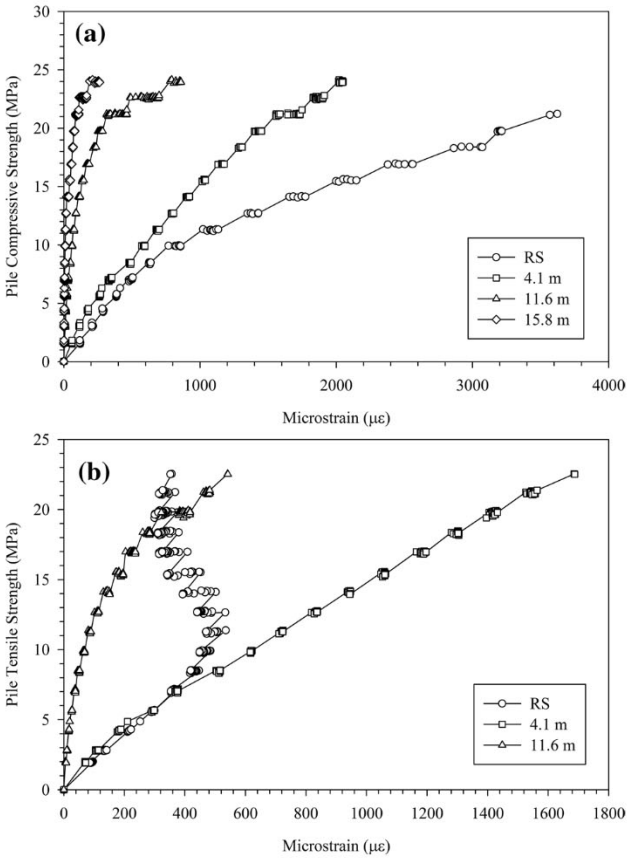

Fig. 11 Stress–strain responses from "sister" bars for **a** MC micropile and **b** MT micropile

is that the load test interval that corresponds to a pile compressive stress between 10 to 18 MPa has a total deformation of about 2300 με in the reference section. Additionally, a deformation equal to 940 με was caused during the load-holding periods. In other words, 40% of the total deformation developed during the loading interval was related to the micropile cross-section creep response of the reference level. It is likely that that the severe creep mechanism at the RS indicated a localized neat cement grout plastification at the micropile's head since the samples of neat cement grout tested in the laboratory presented low compressive strength and deformation modulus (f_{c28} = 15 MPa; E_{grout} = 6 GPa) as well as intense shrinkage. Indeed, the unconfined compressive strength of the grout material at 28 days was below the values recommended by FHWA [1], NBR 6122 [56] and EN 14,199 [57] (20 MPa, 28 MPa, 25 MPa, respectively). The MT micropile presented an atypical behavior at the first instrumentation level after a pile uplift stress of 6 MPa at the top of the micropile as shown in Fig. 11. From this value, the strain induced by the applied loads tended to decrease during the load-holding periods rather than increase or stabilize indicating a strain gauge malfunction at this level.

The axial load transfer was obtained by the procedure described by Fellenius [58] also called the tangent/secant methodology. This method is suitable for composite piles since it considers the inherently nonlinear and inelastic stress–strain response of the grout material [9, 59–62]. The nonlinearity behavior of the MC and MT micropiles is indicated in Fig. 11. In other words, composite piles present a degradation in their deformation modulus over large stress imposed in a static load test. Fellenius [58] derived the secant pile modulus from the tangent modulus line in order to determine the stress for a particular induced strain in a specific "sister" bar section. The tangent modulus line represents the rate of decay of the pile deformation modulus, as a composite structure, under an increased stress–strain, when the shaft resistance above the gage location has been fully mobilized. It is obtained by plotting the load increment divided by the strain increment versus strain. Based on Fellenius [58], the lines and curves are expressed as follows in Eq. (5):

$$E_t = \frac{d\sigma}{d\varepsilon} = A\varepsilon + B \tag{5}$$

where E_t is the tangent modulus, σ is the applied stress; $d\sigma = (\sigma_{n+1} - \sigma_n)$ is the change of stress from one load increment to the next, ε is the induced strain (microstrain, με), $d\varepsilon = (\varepsilon_{n+1} - \varepsilon_n)$ is the change of strain from one load increment to the next, A is the slope of the tangent modulus line (modulus degradation or rate of decay) and B is the initial tangent modulus.

Equation (6) is obtained by integrating Eq. (5) for the composite pile behavior, which results in:

$$\sigma = 0.5A\varepsilon^2 + B\varepsilon \tag{6}$$

The stress in a specific micropile cross-section level for an induced strain is shown in Eq. (7), where E_s is the secant pile modulus, given by Eq. (8).

$$\sigma = E_s\varepsilon \tag{7}$$

$$E_S = 0.5A\varepsilon + B \tag{8}$$

Figure 12 presents the tangent modulus versus strain diagram of the studied micropiles. Figure 12a shows that the three uppermost instrumented sections of the micropile under compression load (SR, 4.1 m and 11.6 m) converged to a straight line after a deformation of 500 με. At this point, all shaft resistance from the reference section to a depth of 11.6 m has been fully mobilized. In other words, this line represents the tangent modulus of a free column with the same properties of the composite pile without the effects of the surrounding soil. Linear regression of the slope of the MC micropile tangent-modulus line (Best Fit Line) provides the A and B coefficients of Eq. (5). The average initial tangent modulus of the micropile under compression

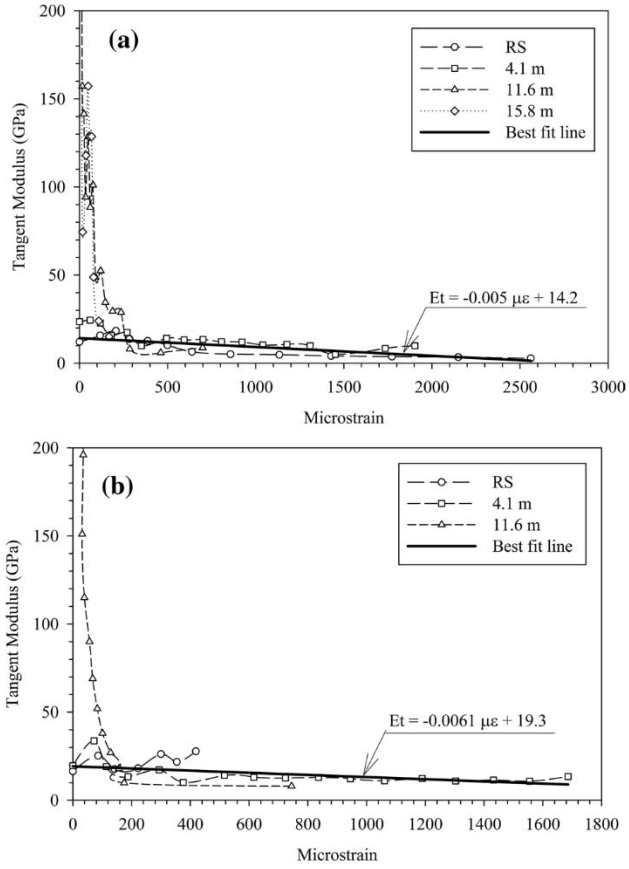

Fig. 12 Tangent modulus for **a** MC micropile and **b** MT micropile

was 14.2 GPa, and the slope of the tangent line (rate of decay) was − 0.005 GPa per microstrain. Closer inspection in Fig. 12a shows that the last gauge level (15.8) also mobilized a significant shaft resistance and tended to step into the Best Fit Line. Therefore, it can be inferred that all shaft resistance of the MC micropile was close to being fully mobilized. Figure 12b indicates that all instrumented sections of the MT micropile converged to a straight line after a deformation of 250 με. As a result, all shaft resistance above the third gauge level was fully mobilized (first and second pile segment). Besides, the first "sister" bar indicated an unconventional behavior after this deformation level, probably related to strain gauge malfunction. The average initial tangent modulus for MT was equal to 19.3 GPa and the rate of decay was − 0.0061 GPa per microstrain. The highest value of the initial tangent modulus regarding the MT micropile was already expected due to the presence of the additional threaded mono bars centrally installed for the load test conduction purpose, which increased the overall stiffness of the micropile.

By inserting the values of A and B into Eq. (8) and then using Eq. (7), it is possible to compute the average stress in the pile over the length. Furthermore, by multiplying Eq. (7) by the pile's cross-section area, it gives the load distribution of the instrumented pile subjected to a static loading test as it can be seen in Fig. 13.

Figure 13a shows that all load applied at the top of the pile is mainly dissipated through lateral resistance. Further analysis shows that after the load stage of 1400 kN, the load transfer diagram has its shape modified, especially at the third pile segment, indicating the beginning of tip mobilization due to the eminent saturation of the lateral resistance. Indeed, the load–movement response also presented a substantial increase in the slope after this loading stage (Fig. 10), which indicates the threshold between the full mobilization of the shaft resistance and the development of tip resistance. Just before the first plunging failure, tip resistance assumes a value of 7% of the applied load at the pile's head (P_{tip} = 119 kN) considering a tip diameter equal to the drilled hole (Db = 0.3 m). Thus, the evaluation of the tip resistance throughout the loading stages in a static load test evidenced to be an effective method for determining the ultimate ground-to-grout capacity of a micropile as emphasized by Han and Ye [30]. Additionally, the preliminary design for the axial geotechnical capacity proposed by the FHWA [1], presented a good fit for the new micropile and tropical soil conditions since the calculated value (PG_{ult} = 1560 kN) was near the ultimate load capacity of the micropile ($P_{SMLT,c}$ = 1581 kN), excluding the tip resistance.

From Fig. 13b, after the loading stage of 300 kN, the load transfer mechanism did not occur properly to a depth of 4 m, approximately. As the neat cement grout presented low mechanical properties, the effective interface contact between the annulus grout and the surrounding soil was probably lost due to excessive cracking under tension/shear stresses at the upper region of the pile, which reduced the axial load transfer efficiency at the soil–pile interface. As a result, after the load stage of 600 kN, all applied load at the top of the pile was absorbed by its structural cross section instead of transferring part of it to the surrounding soil, i.e., the pile segment from the ground level to a depth of 4 m behaved as a free-length section. This phenomenon is also called debonding of micropile as stated by Gómez et al. [27], and it happens when the soil–pile interface is not able to retain significant shear strength after a post-peak behavior, i.e., it behaves in a brittle manner (shear resistance decreases after failure). The remaining bond length (4–17 m) presented a nonlinear behavior of axial load distribution until a load stage of 1400 kN. After that point, the load-transfer response changes to a nearly linear behavior which indicates the development of a constant bond unit stress on the bond zone. According to Holman and Barkauskas [9], this phenomenon can be an indicative of the micropile's failure. Indeed, a pullout failure occurred at 1600 kN. Finally, considering that the MT micropile developed its entire resistance through grout-to-ground bond resistance, the method

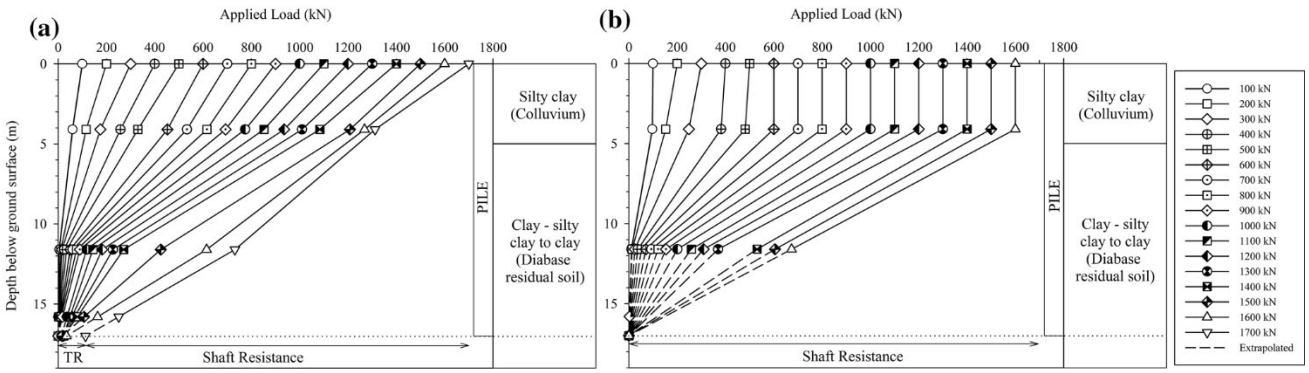

Fig. 13 Load distribution along depth for **a** MC micropile and **b** MT micropile

suggested by the FHWA [1] also presented a good fit since the calculated ultimate geotechnical capacity was notably close to that experienced in the field test ($P_{SMLT,t}$ = 1600 kN).

It is apparent that the micropiles under compression and tension loads behave similarly in terms of shaft load capacity even though previous studies found otherwise [30–32, 37]. They experienced shaft tension load capacities to be lesser than the compression load capacity. Hence, the explanation for the MT micropile to reach a value of the same magnitude of the compression micropile relies on (1) the number of post-grouting phases, (2) the number of valves opened in deep higher resistant soil stratum and (3) the higher cement consumption during pile installation. The MT micropile had two phases of post-grouting treatment at the third pile segment instead of one as the MC micropile and a cement consumption of 2.6 times greater in this region than the micropile under compression which probably strengthened the surrounding ground stratum and improved the grout-to-ground interface under tension loads (see Table 1).

Grout-to-ground bond unit stress

The grout-to-ground bond unit stress (τ) along the shaft of the micropile between two levels of strain gages can be computed as follows in Eq. (9):

$$\tau = \frac{\Delta P}{\pi D l} \tag{9}$$

where ΔP is the load difference between two consecutive gauge levels, l is the distance between two consecutive gauge levels and D is the diameter of the friction interface, which in this study was considered equal to the diameter of the drill hole (D_b = 0.3 m). Figure 14 illustrates the distribution of the grout-to-ground bond unit stress along the shaft for the MT and MC micropiles. It also presents the ultimate skin friction (f_s) obtained by the traditional α method. The ultimate skin friction through this method is computed based on Eq. (10) as follows:

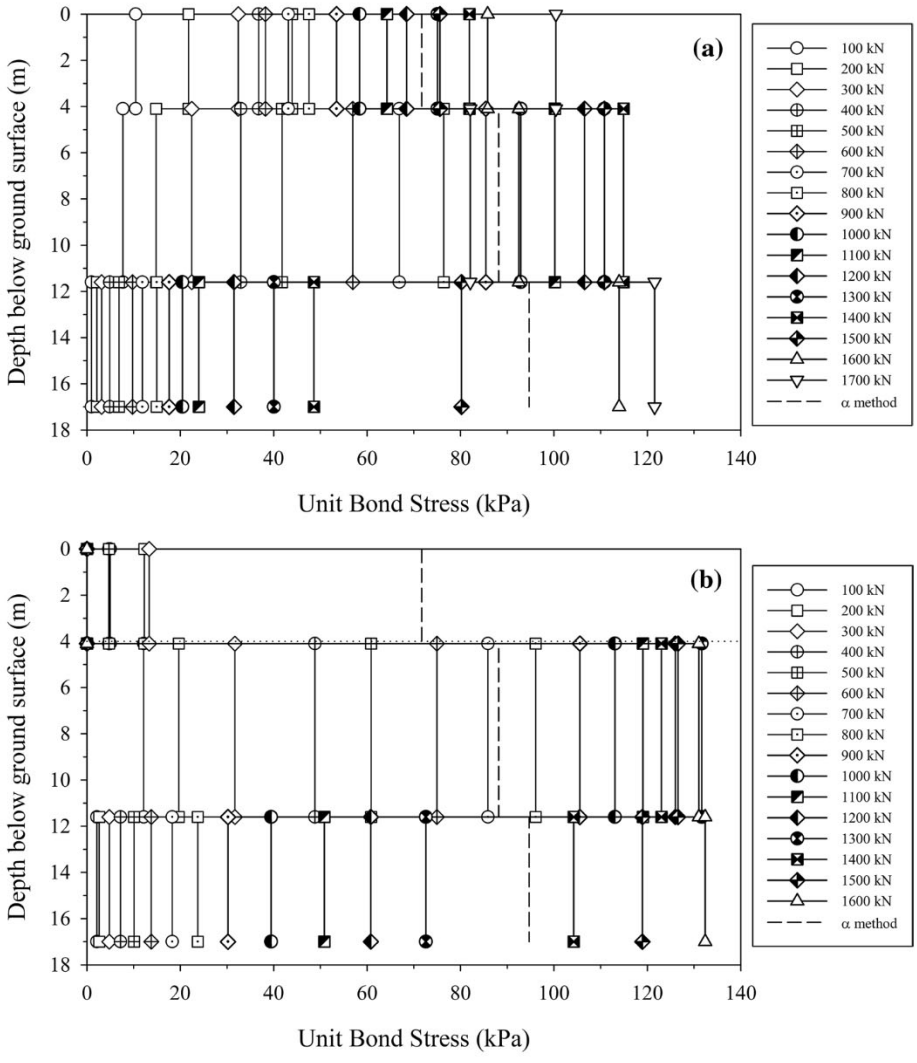

Fig. 14 Distribution of unit bond stress of the micropile along depth **a** MC micropile; and **b** MT micropile

$$\tau = \alpha c_u \tag{10}$$

where c_u is the undrained shear resistance of the soil (average values calculated by Eq. 1 for each instrumented section), and α is the empirical coefficient according to API [63], which are:

$\alpha = 1 - \frac{c_u - 25}{90}$, if $25\,\text{kPa} < c_u < 70\,\text{kPa}$;

$\alpha = 1$, if $c_u \leq 25\,\text{kPa}$;

$\alpha = 0.5$, if $c_u \geq 70\,\text{kPa}$.

Figure 14a shows that in general the unit bond stress increased at each load stage increment at the SMLT. However, there was an unconventional behavior in the MC micropile at higher loads. When changing the load stage from 1400 to 1500 kN, the unit bond stress of the first (0–4.1 m) and the second (4.1–11.6 m) segments decreased instead of increasing or stabilizing, indicating a soft-strain behavior at the soil–pile interface. Additionally, the unit bond stress almost doubled in the last section (from 48 kPa at a load stage of 1400 kN to 80 kPa at a load stage of 1500 kN), showing a considerable increase in the load transfer mechanism in this region due to the post-peak behavior of the upper layers. The post-peak softening of the mobilized bond strength for soil–grout interfaces has also been observed by Gómez et al. [27], Wen et al. [32], Chu and Yin [64], Hossain and Yin [65].

The micropile under tension loads also developed a post-peak reduction of the mobilized bond stress as it can be noted in Fig. 14b. It firstly occurred in the first pile segment (0–4.1 m) under the load stage of 300 kN as previously mentioned. This phenomenon directly affected the load-transfer mechanism in the upper segment of the pile since the unit bond stress decreased from 13 kPa to 0 after the load stage of 600 kN. After this load step, the first pile segment behaved as a free-length section. The second post-peak event happened during the change of the loading stage from 1300 to 1400 kN at the second pile segment (4.1–11.6 m). The mobilized unit bond stress was reduced from 131 to 123 kPa. Additionally, the unit shaft resistance had a considerable increase in the last section (from 73 kPa at a load stage of 1300 kN to 104 kPa at a load stage of 1400 kN) due to the post-peak behavior of the upper layer.

The aforementioned post-peak softening behavior on the soil–pile interface of both micropiles is better visualized in the plot of mobilized unit bond stress versus shaft relative movement presented in Fig. 15. The relative shaft movement at each pile segment was approximately estimated by Eqs. (11) to (14) as follows:

$$\delta_{n1} = \rho_0 - \Delta_{e1} \tag{11}$$

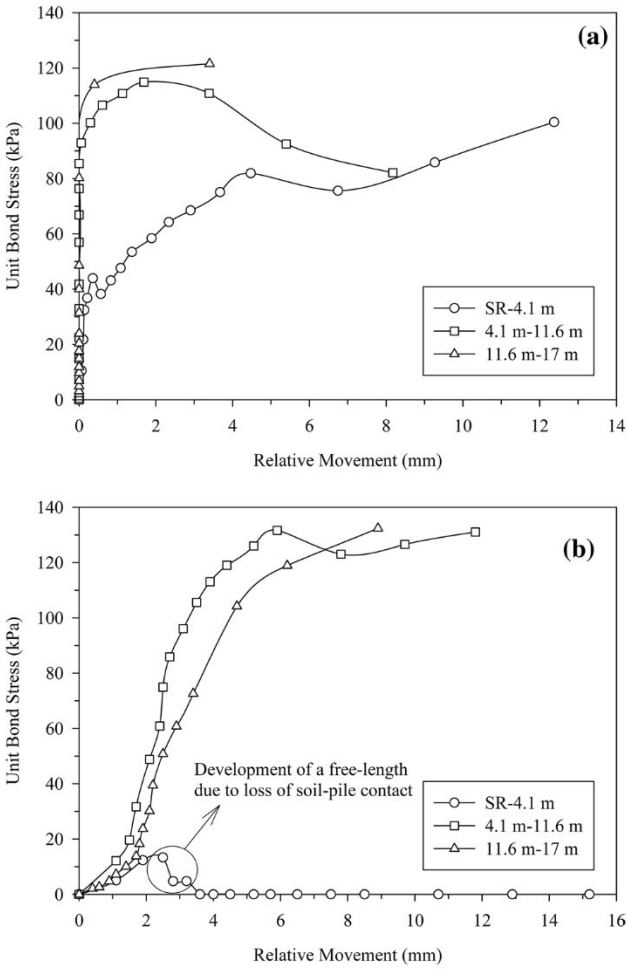

Fig. 15 Unit bond stress versus relative movement for **a** MC micropile and **b** MT micropile

$$\delta_{n2} = \rho_0 - \Delta_{e1} - \frac{\Delta_{e2}}{2} \tag{12}$$

$$\delta_{n3} = \rho_0 - \Delta_{e1} - \frac{\Delta_{e2}}{2} - \frac{\Delta_{e3}}{2} \tag{13}$$

$$\Delta_{e2} = \frac{P_i + P_f}{2E_{sec}A_{pile}}l \tag{14}$$

where δ_{n1}, δ_{n2} and δ_{n3} are the relative shaft movement of the first, second and third pile segments, respectively, ρ_0 is the pile head movement, Δ_{e1}, Δ_{e2}, Δ_{e3} is the elastic shortening of the first, second and third pile segments, respectively, P_i is the load at the top of a pile segment, P_f is the load at the bottom of a pile segment, E_{sec} is the average secant modulus of pile segment obtained by Eq. (8), A_{pile} is the pile cross-section area assuming a diameter equal to the drilled hole

(Db = 0.3 m) and l is the distance between two consecutive gauge levels from Eq. (9).

Figure 15 shows a particular behavior of the relationship between the unit bond stress and micropile–soil relative displacement for each soil layer under a specific type of loading. Regarding the first pile segment, the unit bond stress under compression presented two brittle failures (at 44 kPa and at 82 kPa), and after the second one, it presented a hardening behavior. Meanwhile, for the same pile segment, the unit bond stress under tension showed that after a maximum value of 13 kPa, it gradually decreased to a zero residual value. Figure 15a shows that the unit bond stress of the second segment presented a considerable post-peak softening of the unit bond stress (from 115 to 82 kPa), while Fig. 15b shows that the post-peak reduction of the unit bond stress under tension was smoother. Finally, the unit bond stress of the third pile segment under compression indicates a tendency to a elastoplastic behavior with an ultimate value close to 120 kPa, while the unit bond stress under tension for the last segment shows a hardening behavior after 100 kPa with a maximum value of 132.5 kPa before the first plunging failure of the MT micropile.

These results are likely to be related to the sudden failure of both micropiles during the SMLT as they also presented a post-peak reduction in the load–movement response after the first plunging failure, indicating a residual value of 1350 kN for the micropile under compression and 1300 kN for that under tension (see Fig. 10). It can be suggested that the post-peak softening behavior of the unit bond stress in micropiles under high loading conditions may cause abrupt and unexpected failure mechanisms at the top of post-grouted micropiles. A possible explanation for this might be that the samples of neat cement grout presented intense shrinkage which could have triggered the instabilities in the soil–grout interface. Therefore, the use of anti-shrinkage additives is recommended for this type of micropile, especially at the annulus grout–steel pipe interface, to reduce or even avoid a brittle response.

The ultimate bond strength of both soil layers is computed and presented in Table 4. It can be noted that the ultimate bond strength under tension is higher than that under compression for the diabase residual soil layer. To this extent, the average ultimate bond strength under tension load for this layer is approximately 1.12 times that under compression load. Furthermore, the ratio of the ultimate bond strength under compression to that under tension, considering the entire bond length of the pile (Lb = 17 m), is close to 1.0. Han and Ye [30] observed a ratio of 1.75 for type B micropiles and Wen et al. [32] a ratio of 1.71 for type C micropiles. Both studies were performed in cohesion soils with an average undrained soil strength throughout the pile's shaft of 29 kPa for the first study and 50 kPa for the second one. The higher ultimate bond strength under tension load and, consequently, the lower ratio of $|\tau u/\tau' u|$ may be explained by the post-grouting methodology used in the present study (type D according to FHWA [1]). As the micropile under tension loads was performed with more than one post-grouting phase and with higher cement consumption and injection pressure in the deep resistant stratum (average cu of 95 kPa), the soil–pile bond resistance under tension was enhanced. Therefore, it can be stated the ultimate grout-to-ground bond strength under tension loads can be improved with the grouting technology presented in this study.

The average value of ultimate bond strength of the micropile under compression is in the range of the values obtained by Jeon and Kulhawy [33] for type C and D micropiles. These authors found a range of 77.5 –109 kPa for silty clay soils with an average undrained shear strength of 170 kPa (London Clay). On the other hand, the average value of the ultimate bond strength under tension is close to the range obtained by Misra et al. [66, 67] for type D micropiles under uplift loads. According to these studies, the average ultimate bond strength was between 113 and 151 kPa for medium to dense silty clay of medium to high plasticity. Therefore, the values of ultimate bond strength obtained in the present study are close to the values of other experimental studies of post-grouted micropiles embedded in silty clay soils.

It can be observed that the recommended values by the FHWA [1] are close to the test result with an estimated/measured ratio of 0.98 indicating a good fit for preliminary design conditions for the new micropile embedded in

Table 4 Ultimate bond strength of each soil layer

Soil types	UNICAMP results			Recommended values (kPa)	
	Ultimate bond strength (kPa)			FHWA [1]	API [63]
	MC (τ_u)	MT (τ'_u)	MC/MT (τ_u/τ'_u)		
Silty clay (colluvium)	100	–	–	50–145	75
Silty clay to clay (diabase residual soil)	118	132	0.89	50–145	91
Average value	99	100	0.99	97.5	83

Average value is the ultimate average unit bond stress along the entire bond length (Lb = 17 m)

tropical lateritic soil. Moreover, the values recommended by the API [63] for conventional nongrouted piles are lower than values measured in the field test. These results suggest that the post-grouting technique probably enhanced the grout-to-ground bond strength along the pile shaft. To this extent, the ultimate bond stress of the silty clay (colluvium) is improved by 33%, while the diabase residual soil layer is improved by 29%, both under compression load. Moreover, the ultimate bond stress of the diabase residual soil is improved by 45% under tension load. These results reflect those of Wen et al. [32] who also found that post-grouting techniques played an important role in improving the soil–pile interface of micropiles embedded in marine soft clay.

Finally, the ultimate grout-to-ground bond strength under compression and under tension is higher than the average values of lateral resistance obtained by Albuquerque et al. [41] for other types of nondisplacement piles embedded in tropical lateritic soil (Experimental Site I shown in Fig. 1). Based on these authors, the average maximum lateral resistance of bored piles was 41 kPa, while the average value for continuous flight auger (CFA) was 57 kPa. According to these data, we can infer that the two-step grouting methodology with high injection pressures used in this study significantly enhanced the lateral resistance at the soil–pile interface of the micropiles. The average ultimate bond strength is 2.41 and 1.75 times greater than the maximum average lateral resistance measured for traditional bored and CFA piles, respectively. As a result, the type D post-grouting methodology showed to be essential in improving the load capacity of the micropiles installed in tropical lateritic soil.

Summary and conclusions

In this study, a new configuration of post-grouted steel pipe micropiles was installed in a tropical lateritic soil at a new experimental site localized at the University of Campinas, Brazil. In short, the main innovation of the new construction technology is the use of a high-capacity steel tube as casing protection, drilling tool, injection device and structural element. Furthermore, the micropiles were performed with a two-step process of grouting with high injection pressures which positively affected their overall bearing capacity. Therefore, they can be treated as a special type of micropile and also be classified as a type D based on the grouting methodology, according to FHWA [1]. Full-scale pile loading tests were performed to investigate the axial behavior under compression and tension of the new set of micropiles. Aspects such as the difference between shaft bearing capacity and grout-to-ground bond strength under both load conditions were analyzed and discussed based on the interpretation of the load–movement response and the instrumentation data. The main conclusions can be drawn, as follows:

- Slow monitored load test results indicated a sudden failure after the full mobilization of the grout-to-ground bond strength of both micropiles. This indicates that the lateral resistance governs the overall bearing capacity of the presented micropiles, and tip resistance should not be considered for workload or ultimate load conditions;
- The ultimate shaft capacity of the micropile under tension was almost the same as the micropile under compression loads, excluding tip capacity. In this instance, the preliminary design computation of the ultimate capacity of type *D* micropiles, suggested by the FHWA [1], provided a close estimation of the ultimate load for both piles;
- The tangent/secant method proposed by Fellenius [58] is indicated to be appropriate for instrumentation data interpretation of the studied micropiles in view of the nonlinear behavior of their composite structure;
- Both micropiles presented a post-peak softening behavior of the mobilized bond stress along the shaft which reflected in a brittle response of the load–movement response at the top of the pile. The sensitive response of the annulus grout and the steel pipe interface was probably due to the intense shrinkage of the neat cement grout used during the grouting phases. Although the use of anti-shrinkage additives for this type of micropile was recommended to overcome this issue, the precise mechanism of the post-peak reduction of the mobilized bond stress remains to be elucidated in further studies;
- The average value of the ultimate bond strength suggested by the FHWA [1] for type D micropiles was in good agreement with the values measured in the field for both types of loads, showing an estimated/measured ratio close to the unity. The average value of the ultimate bond strength under tension was of the same magnitude as the under compression, which indicates the effectiveness of the micropile installation methodology on the ground-to-grout bond tension resistance enhancement;
- The two-step grouting technique with higher injection pressures showed to positively affect the axial bearing capacity of the steel pipe micropiles embedded in diabase residual soil since the values of ultimate bond strength predicted by the API [63] for nongrouted piles were improved by 29% and 45% under compression and tension loads, respectively, for this type of soil. In addition, the average ultimate grout-to-ground bond strength of the micropiles under compression and tension is 2.41 and 1.75 times greater than the average lateral resistance of traditional nongrouted and non-injected piles performed in the same soil conditions at Unicamp,

respectively. Therefore, these results also indicate that the presented grouting methodology leads to a lateral resistance improvement of the tropical lateritic soil and the micropile interface.

Acknowledgements The authors gratefully acknowledge the support of the University of Campinas (Unicamp) and INCOTEP Anchoring Systems for the construction of the new experimental site and the National Council for the Improvement of Higher Education (CAPES) for the scholarships granted to the post-graduate students participating in the study.

Availability of data, material and code All data, materials and code generated or used during the study appear in the published article.

Compliance with ethical standards

Conflict of interest On behalf of all authors, the corresponding author states that there is no conflict of interest.

References

1. FHWA (2005) Micropile design and construction—reference manual. FHWA, Washington, DC, Rep. No. FHWA NHI-05-039
2. Thorburn S, Hutchison JF (1985) Underpinning. Surrey University Press, Glasgow and London
3. Bruce DA, Juran I, Dimillio AF (2001) High capacity grouted micropiles: the state of practice in the United States. In: Proceedings of international conference on soil mechanics and geotechnical engineering, Rotterdam, Netherlands, pp 851–854
4. Lizzi F (1982) The pali radice (root piles). In: Symposium on soil and rock improvement techniques including geotextiles, reinforced earth and modern piling methods, Bangkok, paper D-3
5. Cadden A, Gómez J, Bruce D, Armour T (2004) Micropiles: recent advances and future trends. In: Proceedings of current practices and future trends in deep foundations, Los Angeles, pp 140–165
6. Russo G (2004) Full-scale load tests on instrumented micropiles. Proc Inst Civ Eng Geotech Eng 157(3):127–135. https://doi.org/10.1680/geng.2004.157.3.127
7. Tsukada Y, Miura K, Tsubokawa Y, Otani Y, You GL (2006) Mechanism of bearing capacity of spread footings reinforced with micropiles. Soils Found 46(3):367–376. https://doi.org/10.3208/sandf.46.367
8. Han J, Ye SL (2006a) A field study on the behavior of a foundation underpinned by micropiles. Can Geotech J 43(1):30–42. https://doi.org/10.1139/t05-087
9. Holman PT, Barkauskas DB (2007) Mechanics of micropile performance from instrumented load tests. In: Proceedings of 7th international symposium on field measurements in geomechanics, Boston
10. Larsson K, Jog D (2014) Performance of micropiles used to underpin highway bridges. J Perform Constr Facil 28(3):592–607. https://doi.org/10.1061/(ASCE)CF.1943-5509.0000426
11. El Kamash W, Han J (2016) Numerical analysis of existing foundations underpinned by micropiles. Int J Geomech 17(6):04016126. https://doi.org/10.1061/(ASCE)GM.1943-5622.0000833
12. Bruce DA, Chu EK (1995) Micropiles for seismic retrofit, proceedings. In: Proceedings of national seismic conference on bridges and highways, San Diego, California
13. Chen Y, Zhang Z, Liu H (2017) Study of the seismic performance of hybrid A-frame micropile/MSE (mechanically stabilized earth) wall. Earthq Eng Eng Vib 16(2):275–295. https://doi.org/10.1007/s11803-017-0382-0
14. Mashhoud HJ, Yin JH, Panah AK, Leung YF (2020) A 1-g shaking table investigation on response of a micropile system to earthquake excitation. Acta Geotech 15(4):827–846. https://doi.org/10.1007/s11440-018-0742-6
15. Haddad ED, Choobbasti AJ (2019) Response of micropiles in different seismic conditions. Innov Infrastruct Solut 4(1):53. https://doi.org/10.1007/s41062-019-0226-z
16. Pinyol NM, Alonso EE (2012) Design of micropiles for tunnel face reinforcement: Undrained upper bound solution. J Geotech Geoenviron Eng 138(1):89–99. https://doi.org/10.1061/(ASCE)GT.1943-5606.0000562
17. Moayed RZ, Naeini SA (2012) Improvement of loose sandy soil deposits using micropiles. KSCE J Civ Eng 16(3):334–340. https://doi.org/10.1007/s12205-012-1390-2
18. Esmaeili M, Nik MG, Khayyer F (2013) Experimental and numerical study of micropiles to reinforce high railway embankments. Int J Geomech 13(6):729–744. https://doi.org/10.1061/(ASCE)GM.1943-5622.0000280
19. Sun SW, Zhu BZ, Wang JC (2013) Design method for stabilization of earth slopes with micropiles. Soils Found 53(4):487–497. https://doi.org/10.1016/j.sandf.2013.06.002
20. Xiang B, Zhang LM, Zhou LR, He YY, Zhu L (2015) Field lateral load tests on slope-stabilization grouted pipe pile groups. J Geotech Geoenviron Eng 141(4):04014124. https://doi.org/10.1061/(ASCE)GT.1943-5606.0001220
21. Bayesteh H, Sabermahani M (2018) Full-scale field study on effect of grouting methods on bond strength of hollow-bar micropiles. J Geotech Geoenviron Eng 144(12):04018091. https://doi.org/10.1061/(ASCE)GT.1943-5606.0001983
22. Gouvenot D, Gabaix JC (1975) A new foundation technique using piles sealed by cement grout under high pressure. In: Proceedings of 7th annual offshore technology conference, Dallas, Texas
23. Bustamante M, Doix B (1985) Une méthode pour le calcul des tirants et des micropieux injectés. Bulletin de Liaison des Laboratoires des Ponts et Chaussés 140:75–92
24. Barley AD, Windsor CR (2000) Recent advances in ground anchor and ground reinforcement technology with reference to the development of the art. In: ISRM international symposium, Melbourne, Australia
25. Wan Z, Dai G, Gong W (2018) Full-scale load testing of two large-diameter drilled shafts in coral-reef limestone formations. Bull Eng Geol Environ 77(3):1127–1143. https://doi.org/10.1007/s10064-017-1206-1
26. Wan Z, Dai G, Gong W (2019) Field study on post-grouting effects of cast-in-place bored piles in extra-thick fine sand layers. Acta Geotech 14(5):1357–1377. https://doi.org/10.1007/s11440-018-0741-7
27. Gómez J, Cadden A, Bruce DA (2003) Micropiles founded in rock. Development and evolution of bond stresses under repeated loading. In: Proceedings of 12th Panamerican conference on soil mechanics and geotechnical engineering, Cambridge
28. Seo H, Prezzi M, Salgado R (2013) Instrumented static load test on rock-socketed micropile. J Geotech Geoenviron Eng 139(12):2037–2047. https://doi.org/10.1061/(ASCE)GT.1943-5606.0000946
29. Jang YE, Han JT (2018) Field study on axial bearing capacity and load transfer characteristic of waveform micropile. Can Geotech J 55(5):653–665. https://doi.org/10.1139/cgj-2017-0155
30. Han J, Ye SL (2006b) A field study on the behavior of micropiles in clay under compression or tension. Can Geotech J 43(1):19–29. https://doi.org/10.1139/t05-089

31. Qian Z, Lu X (2011) Behavior of micropiles in soft soil under vertical loading. Adv Mater Res 243–249:2143–2150. https://doi.org/10.4028/www.scientific.net/AMR.243-249.2143
32. Wen L, Kong G, Li Q, Zhang Z (2020) Field tests on axial behavior of grouted steel pipe micropiles in marine soft clay. Int J Geomech 20(6):06020006. https://doi.org/10.1061/(ASCE)GM.1943-5622.0001656
33. Jeon SS, Kulhawy FH (2001) Evaluation of axial compression behaviour of micropiles. In: Proceedings of a speciality conference: foundations and ground improvement, pp 460–471
34. Sabermahani M, Nasr M, Elahi H (2012) Study on soil type effects on micropile behavior using full scale loading tests. In: GeoCongress 2012: state of the art and practice in geotechnical engineering, pp 2678–2687. https://doi.org/10.1061/97807844121.274
35. Abd Elaziz AY, El Naggar MH (2012) Axial behaviour of hollow core micropiles under monotonic and cyclic loadings. Geotech Test J 35(2):249–260. https://doi.org/10.1520/GTJ103880
36. Abd Elaziz AY, El Naggar MH (2014) Geotechnical capacity of hollow-bar micropiles in cohesive soils. Can Geotech J 51(10):1123–1138. https://doi.org/10.1139/cgj-2013-0408
37. Carvalho D, Matilla JD, Albiero J, Cintra JCA (1991) Tension and compression load tests on root-type instrumented piles. In: Proceedings of seminar of engineering and special foundations, São Paulo, Brazil. (in Portuguese)
38. Carvalho D, Cintra JCA (1995) Aspects of the bearing capacity of root piles in some Brazilian soils. In: Proceedings of 2nd international seminar—deep foundations on bored and auger piles, Belgica
39. Choi C, Cho SD (2010) Field verification study for micropile load capacity. In: Proceedings of 10th international workshop on micropiles, Washington, DC, United States
40. Drbe OFEH, El Naggar MH (2015) Axial monotonic and cyclic compression behaviour of hollow-bar micropiles. Can Geotech J 52(4):426–441. https://doi.org/10.1139/cgj-2014-0052
41. Albuquerque PJR, Massad F, Fonseca AV, Carvalho D, Santos J, Esteves EC (2011) Effects of the construction method on pile performance: evaluation by instrumentation—part 1: experimental site at the State University of Campinas. Soils Rocks 34:35–50
42. Garcia JR, Albuquerque PJR (2019) Analysis of the contribution of the block-soil contact in piled foundations. Latin Am J Solids Struct 16:1–22. https://doi.org/10.1590/1679-78255565
43. Albuquerque PJR, Carvalho D, Kassouf R, Fonte NL (2019) Behavior of laterally top-loaded deep foundations in highly porous and collapsible soil. J Mater Civ Eng 31:04018373. https://doi.org/10.1061/(ASCE)MT.1943-5533.0002582
44. Freitas Neto O, Cunha RP, Albuquerque PJR, Garcia JR, Santos Junior OF (2020) Experimental and numerical analyses of a deep foundation containing a single defective pile. Latin Am J Solids Struct 17:1–15. https://doi.org/10.1590/1679-78255827
45. Albuquerque PJR, Carvalho D, Massad F (2005) Bored, continuous flight auger and omega instrumented piles: behavior under compression. In: Proceedings of 16th international conference on soil mechanics and geotechnical engineering, vol 16, No. 4, pp 2075–2078. https://doi.org/10.3233/978-1-61499-656-9-2075
46. Albuquerque PJR, Rodriguez TG (2016) Assessment of results of CPT tests in porous lateritic unsaturated soil from Campinas, Brazil. In: Proceedings of 5th international conference on geotechnical and geophysical site characterization, Gold Coast, v.1, pp 1–6
47. Miguel MG, Albuquerque PJR, Azevedo GS, Silva GSV, Carvalho D (2007) Lateritic behaviour of the colluvial soil from Campinas-SP-Brasil. In: Proceedings of thirteen pan-American conference on soil mechanics and geotechnical engineering, Isla de Margarita
48. Albuquerque PJR, Carvalho D, Fontaine RB (2008) Evaluation of the lateral friction of piles in a diabasic soil through pressuremeter test. In: Proceedings of international site characterization, Taipei
49. Carvalho D, Albuquerque PJR (2013) Uplift behavior of bored piles in tropical unsaturated sandy soil. In: Proceedings of 18th international conference on soil mechanics and geotechnical engineering, Paris, pp 2707–2710
50. Peixoto ASP, Albuquerque PJR, Carvalho D (2000) Utilization of SPT-T, CPT and DMT tests to predict the ultimate bearing capacity of precast concrete pile in Brazilian unsaturated residual soil. In: Advances in unsaturated geotechnics, pp 32–39. https://doi.org/10.1061/40510(287)3
51. Robertson PK (2009) Interpretation of cone penetration tests—a unified approach. Can Geotech J 46(11):1337–1355. https://doi.org/10.1139/T09-065
52. ASTM (2017) Standard practice for classification of soils for engineering purposes (Unified Soil Classification System). West Conshohocken, PA, ASTM D2487-17
53. Misra A, Chen CH (2004) Analytical solution for micropile design under tension and compression. Geotech Geol Eng 22(2):199–225. https://doi.org/10.1023/B:GEGE.0000018356.85647.79
54. Misra A, Chen CH, Oberoi R, Kleiber A (2004) Simplified analysis method for micropile pullout behavior. J Geotechn Geoenviron Eng 130(10):1024–1033. https://doi.org/10.1061/(ASCE)1090-0241(2004)130:10(1024)
55. ABNT (2006) Pile static load test—test method. Rio de Janeiro, Brazil, NBR 12131. (**in Portuguese**)
56. ABNT (2019) Piles design and installation. Rio de Janeiro, Brazil, NBR 6122. (**in Portuguese**)
57. British Standard Institution. Execution of special geotechnical work-Micropiles. BS EN 14199
58. Fellenius BH (1989) Tangent modulus of piles determined from strain data. In: The ASCE geotechnical engineering division foundation congress, pp 500–510
59. Fellenius BH, Brusey WG, Pepe F (2000) Soil set-up, variable concrete modulus, and residual load for tapered instrumented piles in sand. In: Performance confirmation of constructed geotechnical facilities, pp 98–114. https://doi.org/10.1061/40486(300)6
60. Finno RJ, Scherer SD, Paineau B (2002) Load transfer characteristics of micropiles in dolomite. In: Proceeding of deep foundations 2002: an international perspective on theory, design, construction, and performance, pp 1038–1053 https://doi.org/10.1061/40601(256)73
61. Deschamps R, Richards T (2005) Installation, measurement, and interpretation of "sister bar" strain gauges in micropiles. In: Proceedings of GEO construction quality assurance/quality control technical conference, pp 167–178
62. Lam C, Jefferis SA (2011) Critical assessment of pile modulus determination methods. Can Geotech J 48(10):1433–1448. https://doi.org/10.1139/t11-050
63. API (1987) Recommended practice for planning, designing and constructing fixed off-shore platforms, Washington, DC
64. Chu LM, Yin JH (2005) Comparison of interface shear strength of soil nails measured by both direct shear box tests and pullout tests. J Geotechn Geoenviron Eng 131(9):1097–1107. https://doi.org/10.1061/(ASCE)1090-0241(2005)131:9(1097)
65. Hossain MA, Yin JH (2012) Influence of grouting pressure on the behavior of an unsaturated soil-cement interface. J Geotech Geoenviron Eng 138(2):193–2002. https://doi.org/10.1061/(ASCE)GT.1943-5606.0000585
66. Misra A, Oberoi R, Kleiber A (1999) Micropiles for seismic retrofitting of highway interchange foundation. In: Proceedings of international workshop on micropiles, Ube City, Japan, pp 215–224
67. Misra A, Roberts LA, Oberoi R, Chen CH (2007) Uncertainty analysis of micropile pullout based upon load test results. J Geotech Geoenviron Eng 133(8):1017–1025. https://doi.org/10.1061/(ASCE)1090-0241(2007)133:8(1017)